Entanglement-assisted, noise-assisted, and monitoring-enhanced quantum bath tagging

Donato Farina
ICFO-Institut de Ciencies Fotoniques, The Barcelona Institute of Science and Technology, Castelldefels, Barcelona 08860, Spain

Vasco Cavina
Complex Systems and Statistical Mechanics, Physics and Materials Science, University of Luxembourg, 1511 Luxembourg, Luxembourg

Marco G. Genoni
Quantum Technology Lab, Dipartimento di Fisica Aldo Pontremoli, Universitá degli Studi di Milano, 20133 Milano, Italy

Vittorio Giovannetti
Laboratorio NEST, Scuola Normale Superiore and Istituto Nanoscienze, CNR, 56127 Pisa, Italy

(Received 1 March 2022; accepted 6 September 2022; published 13 October 2022)

We analyze the capability of discriminating the statistical nature of a thermal bath in the presence of three different types of side resources: prior entanglement between the probing system and an external (dynamically neutral) memory element, the interaction between the probe and an auxiliary bath, and the continuous monitoring of the system mediated by real-time measurements of the auxiliary bath. We discuss in detail how to obtain improved performances in the discrimination by considering different kinds of interactions, i.e., different jump operators, and different monitoring strategies corresponding to continuous homodyne detection and photodetection. We find that the presence of the auxiliary environment can be beneficial, allowing bath discrimination in regimes where in the standard scenario discrimination is not possible. We then show how additionally monitoring this environment, via either continuous homodyne detection or photodetection, is naturally advantageous for quantum bath tagging, in particular in the long-time limit where a large improvement in the discrimination performance is indeed observed. Our approach can in principle be implemented in a circuit QED setup and paves the way to further developments of quantum probing via continuous monitoring.

DOI: 10.1103/PhysRevA.106.042609

I. INTRODUCTION

In quantum metrology and quantum sensing [1–6] a quantum probe is any physical system that allows one to assess the value of an unknown classical parameter that has been "attached" to its state via some dedicated dynamical process. For instance, quantum probes have been used to estimate parameters related either to their Hamiltonian (e.g., a frequency or a coupling constant) or to their unitary evolution (say, a dynamical phase accumulated while moving along a certain trajectory). Quantum probes have also been exploited in order to reconstruct the properties of the surrounding environment [7]; examples are protocols of quantum thermometry [8–18] or aimed to characterize the spectrum of the environment itself [19,20]. More recently, it has been proposed to use a quantum probe to discriminate between thermal baths characterized by different thermal [21] or statistical [22,23] properties. In particular in the latter scenario, a quantum probe S is exploited to determine whether the thermal bath E obeys bosonic or fermionic statistics, a task which hereafter will be referred to as quantum bath tagging (QBT). In such a scheme, S is let to weakly interact with E for some time t and then measured using optimal detection procedures identified by solving the associated quantum hypothesis testing problem [24]. The aim of the present paper is to present a collection of different techniques that can be used to improve the performances reported in [22,23]. The first of such techniques is to allow joint measurements on a compound system SA_1 obtained by adding an external memory element A_1 which, while being dynamically decoupled from the bath E and from the original S, is initially correlated (entangled) with the latter. Similar entangled-assisted detection improvements have been extensively studied in the past (see, e.g., [2,25–31]); here we show that such effects can also be witnessed in the context of QBT procedures. The other two techniques we analyze assume that, while coupled with E and possibly initially correlated with A_1, the probe S can interact with a second auxiliary bath A which, at variance with what happens with E, is assumed to have known statistical and thermodynamic properties. Specifically, we will take A to be a zero-temperature multimode electromagnetic field. Besides allowing us to refer more closely to realistic experimental setups, the role of such an extra environment is twofold: On one hand, the presence of A is used as a way to positively interfere with the S-E coupling in an effort to increase the distinguishability among the quantum trajectories associated with the two hypotheses of the problem (we call this procedure a noise-assisted QBT scheme); on the other hand, A can also be employed to set up an indirect

continuous monitoring of the evolution of S, hence allowing us to acquire information about E in real time and not just at the end of the interaction interval (we call this a monitoring-enhanced QBT scheme). Continuous monitoring of quantum systems [32,33] has indeed been proven useful in the context of quantum metrology: In particular, several works have either discussed the fundamental statistical tools to assess the precision achievable in this framework [34–41] or presented practical estimation strategies [42–57]. The theoretical framework needed to assess hypothesis testing protocols was put forward first by Tsang [58] and then by Kiilerich and Mølmer [59]. We exploit these techniques for our specific aim and we discuss how and when continuous monitoring can be useful for QBT.

In Sec. II we introduce the QBT problem, presenting the physical setup and discussing how to assess hypothesis testing in continuously monitored quantum systems. In Sec. III we show our main results and the modifications we introduce with respect to the original works [22,23] are presented gradually. Considering the elements E, S, and A_1, in Sec. III A we first show that the QBT precision can be enhanced by performing joint measurements on SA_1 under the assumption that the two systems were initialized into a quantum correlated state. Then in Sec. III B we show how the mere presence of the bath A can also help in boosting the QBT procedure. In Sec. III C we finally analyze the advantages one can obtain by using the extra bath A as a method for continuously monitoring the probe dynamics. In Sec. IV we discuss possible implementations of our protocol and draw our conclusions.

II. MODEL

The QBT model we study is schematically sketched in Fig. 1. Apart from E (the thermal environment whose statistical nature we wish to determine) and S (the quantum probe that is put in interaction with E), it includes two extra elements which were not present in the original QBT scheme discussed in Refs. [22,23], namely, an auxiliary bath A whose statistical and thermodynamic properties are assumed to be known and which is also attached to S, and an external quantum memory A_1 that is dynamically decoupled from all the other components of the setup. As in Refs. [22,23], our goal is to decide whether E is a bosonic bath with assigned inverse temperature β_B (hypothesis B) or fermionic with assigned inverse temperature β_F (hypothesis F), the initial priors of these two alternatives being flat. To solve such a task we are allowed to prepare S (which for simplicity we assume to be a qubit) in any desired input configuration, possibly correlated with the memory A_1, let it evolve for some time t, and perform measurements during and/or at the end of the process. The possibility of employing correlated states of S and A_1 was not exploited in Refs. [22,23] and as we will see allows for some useful technical improvements. The main difference of our proposal, however, is the presence of the auxiliary bath A, which we schematize as a zero-temperature multimode electromagnetic (hence bosonic) field. Its role is to induce positive interference effects on the S-E coupling and to permit continuous monitoring in time of the system evolution via photodetection or homodyne measurements (a configuration which may physically correspond to the case where we put S into a dispersive QED cavity).

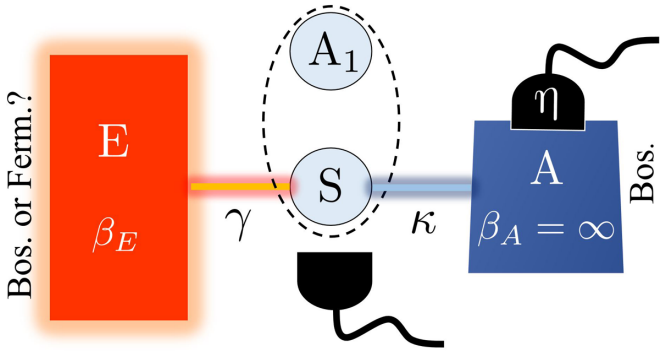

FIG. 1. Schematic representation of the QBT setup. The statistical nature (bosonic or fermionic) of the thermal bath E is determined by studying the modifications it induces on a quantum probe S (a qubit) that has been put in thermal contact with it while interacting with a zero-temperature bosonic auxiliary bath A that is continuously monitored in time via photodetection or homodyne measurements. In the picture γ and κ are the two decay rates of the unconditional evolution of S for the interaction with E and A, respectively, while η is the quantum efficiency of the continuous detection on A. Here A_1 represents a quantum memory that is dynamically decoupled from all the other components of the setup; it can be used to create initial correlations with S which can be monitored via joint measurements on the compound SA_1.

A. Dynamical evolution

In this section we derive the dynamical equations that determine the temporal evolution of the system. Let us start by considering the case where the probe interacts with E and A in the absence of continuous monitoring of the latter. Following Ref. [22], we model the S-E and S-A couplings via a Gorini-Kossakowski-Sudarshan-Lindblad (GKSL) master equation [60,61], a situation realized under the weak-coupling and Markovian hypotheses [62]. Accordingly, defining $\mathcal{D}_{[\hat{\theta}]}$ to be the dissipative superoperator

$$\mathcal{D}_{[\hat{\theta}]}\bullet := \hat{\theta}\bullet\hat{\theta}^\dagger - \tfrac{1}{2}\{\hat{\theta}^\dagger\hat{\theta},\bullet\}, \tag{1}$$

we write the dynamical evolution of the joint density matrix $\hat{\varrho}_q(t)$ of the probe S and the memory A_1 as

$$\frac{d\hat{\varrho}_q(t)}{dt} = \mathcal{L}_q\hat{\varrho}_q(t) + \kappa\mathcal{D}_{[\hat{c}]}\hat{\varrho}_q(t), \tag{2}$$

where the index $q \in \{B,F\}$ is used to specify which hypothesis has been selected for the statistical nature of E. In this equation $\mathcal{L}_q$ is the GKSL dynamical generator which accounts for the free evolution and for the S-E coupling, i.e.,

$$\begin{aligned}\mathcal{L}_q\bullet :=& -i[\hat{H}_S,\bullet] + \gamma[1+s_qN_q(\beta_q)]\mathcal{D}_{[\hat{\sigma}_-]}\bullet \\ &+ \gamma N_q(\beta_q)\mathcal{D}_{[\hat{\sigma}_+]}\bullet,\end{aligned} \tag{3}$$

where $\hat{H}_S := \omega_0\hat{\sigma}_+\hat{\sigma}_-$ is the Hamiltonian of the probe, γ is a positive coupling constant that fixes the timescale of the S-E interaction, and, having set $s_{q=B}=1$ and $s_{q=F}=-1$, $N_q(\beta) := 1/(e^{\beta\omega_0}-s_q)$ is the Bose-Einstein factor (when $q=B$) or Fermi-Dirac factor (when $q=F$): Notice that $\hbar$

has been set equal to 1 and that no free Hamiltonian has been assumed for A_1, which effectively participates in the process only through initial correlations with S that have been possibly established at the beginning of the dynamical evolution. The second term on the left-hand side of Eq. (2) represents instead the S-A coupling with the operator $\hat{c}$ selected depending on the type of interaction one has engineered and with $\kappa \geqslant 0$ being a parameter that gauges its intensity: In particular, setting $\kappa = 0$, we recover the model discussed in Refs. [22,23]. In the following we will consider the two cases $\hat{c} = \hat{\sigma}_-$ and $\hat{c} = \hat{\sigma}_x/2$: The first one corresponds to a purely dissipative model where S loses energy to A via spontaneous emission, while the second choice can be obtained via dispersive coupling that can be engineered, e.g., in circuit-QED systems [63–65].

As already mentioned, Eq. (2) does not include effects associated with a continuous monitoring of A. To account for continuous monitoring we resort to the stochastic master equation (SME) approach of Refs. [32,33]. In particular, we focus on two kinds of measurements, photodetection and homodyne detection with a fixed monitoring efficiency η. In the case of photodetection, under hypothesis q, the corresponding SME for the conditional state of SA_1 reads

$$d\hat{\varrho}^c_q(t) = \mathcal{L}_q\hat{\varrho}^c_q(t)dt + (1-\eta)\kappa\mathcal{D}_{[\hat{c}]}\hat{\varrho}^c_q(t) - \frac{\eta\kappa}{2}\mathcal{H}_{[\hat{c}^\dagger\hat{c}]}\hat{\varrho}^c_q(t)dt + \left(\frac{\hat{c}\hat{\varrho}^c_q(t)\hat{c}^\dagger}{\mathrm{Tr}[\hat{c}\hat{\varrho}^c_q(t)\hat{c}^\dagger]} - \hat{\varrho}^c_q(t)\right)dN_t, \tag{4}$$

where $dN_t \in \{0,1\}$ corresponds physically to the number of photons detected at each time t and mathematically to a Poisson increment defined by its probability of taking value equal to one, $p(dN_t = 1) = \eta\kappa\mathrm{Tr}[\hat{\varrho}^c_q(t)\hat{c}^\dagger\hat{c}]dt$, and we have introduced the superoperator

$$\mathcal{H}_{[\hat{\theta}]}\bullet := \hat{\theta}\,\bullet + \bullet\,\hat{\theta}^\dagger - \mathrm{Tr}[(\hat{\theta}^\dagger + \hat{\theta})\bullet]\,\bullet\,. \tag{5}$$

Similarly, in the case of homodyne detection we obtain the SME

$$d\hat{\varrho}^c_q(t) = \mathcal{L}_q\hat{\varrho}^c_q(t)dt + \kappa\mathcal{D}_{[\hat{c}]}\hat{\varrho}^c_q(t)dt + \sqrt{\eta\kappa}\mathcal{H}_{[\hat{c}]}\hat{\varrho}^c_q(t)dW_t, \tag{6}$$

where the state is conditioned on the continuous output photocurrent

$$dy_t := \sqrt{\eta\kappa}\mathrm{Tr}[\hat{\varrho}^c_q(t)(\hat{c}+\hat{c}^\dagger)]dt + dW_t \tag{7}$$

and dW_t, denoting the difference between the measurement output dy_t and the expected results, mathematically corresponds to a Wiener increment such that the relation $dW_t^2 = dt$ holds deterministically. We remark that by choosing as jump operators the ones defined before, i.e., either $\hat{c} = \hat{\sigma}_-$ or $\hat{c} = \hat{\sigma}_x/2$, we obtain photocurrents (7) with the same form, yielding information on the average value of the operator $\hat{\sigma}_x$. However, the two operators will induce different dynamics, described by the corresponding SME (6).

For both photodetection and homodyne detection strategies, the associated SMEs (4) and (6) can be numerically integrated following the method based on Kraus operators suggested in [66,67] that we review in brief in Appendix A. This results in a collection of quantum trajectories for the conditional density matrix $\hat{\varrho}^c_q(t)$, each identified by a string of records

$$D_t := (x_{t_0+dt}, x_{t_0+2dt}, \ldots, x_{t-dt}, x_t), \tag{8}$$

where we have assumed to perform measurements every infinitesimal time interval dt starting from the initial time t_0 (which we set to zero hereafter) and stopping at time t and for the photodetection and homodyne detection scenarios the x_t correspond to recorded values of either dN_t or dy_t, respectively. It is worth pointing out that, in principle, by averaging over all such solutions, i.e., by averaging $\hat{\varrho}^c_q(t)$ over all the obtained measurement results (8) up to a time t or equivalently by fixing the monitoring efficiency $\eta = 0$, we obtain an unconditional state solution that coincides with the standard master equation (2) of the problem, i.e.,

$$\mathbb{E}[\hat{\varrho}^c_q(t)] = \hat{\varrho}^c_q(t)|_{\eta=0} = \hat{\varrho}_q(t). \tag{9}$$

B. Quantum hypothesis testing in continuously monitored quantum systems

In this section we review the methods that allow us to characterize how efficiently one can solve the QBT problem we are facing. To begin with, consider first the simple case where the data from the continuous monitoring in time are neglected, e.g., by averaging them away or setting $\eta = 0$, a regime in which, due to (9), the evolution of the system is provided by the master equation (2). Having hence selected an input state $\hat{\varrho}(0)$ for the SA_1 system and a total evolution time t, what we have to do is determine whether at the end of the process the state of SA_1 is better described by the density matrix $\hat{\varrho}_B(t)$ or by the density matrix $\hat{\varrho}_F(t)$ obtained by solving Eq. (2) under the two alternative QBT hypotheses. This problem can be easily framed as a special instance of quantum hypothesis testing [24]. Accordingly, we can bound the error probability associated with the selected strategy through the Helstrom inequality

$$p_{\mathrm{err}}[t;\hat{\varrho}(0)] \geqslant \epsilon[t;\hat{\varrho}(0)], \qquad \epsilon[t;\hat{\varrho}(0)] := \frac{1 - \|P_B\hat{\varrho}_B(t) - P_F\hat{\varrho}_F(t)\|_1}{2}, \tag{10}$$

where $\|\bullet\|_1$ denotes the trace norm and P_B and P_F correspond to the prior probabilities for the two events B and F. The threshold value ϵ, conventionally called the Helstrom error probability (HEP), can always be attained via a projective measurement on SA_1 that at time t distinguishes the positive and negative eigenstates of the operator $\Lambda = P_B\hat{\varrho}_B(t) - P_F\hat{\varrho}_F(t)$. In the following we will always consider the scenario where the prior probability distribution is flat, that is, for $P_B = P_F = \frac{1}{2}$, leading to

$$\epsilon[t;\hat{\varrho}(0)] = \frac{1}{2}\left(1 - \frac{\|\hat{\varrho}_B(t) - \hat{\varrho}_F(t)\|_1}{2}\right). \tag{11}$$

In Refs. [22,23] the $\epsilon[t;\hat{\varrho}(0)]$ was used as a bona fide quality factor for the QBT efficiency one can achieve with the selected choice of t and $\hat{\varrho}(0)$. Note, however, that in such works $\hat{\varrho}_B(t)$ and $\hat{\varrho}_F(t)$ referred to the local states of S (i.e., the presence of the external quantum memory A_1 was not allowed) and, most importantly, the auxiliary bath A was not included in the picture [a condition which in our modelization corresponds to setting $\kappa = 0$ in Eq. (2)]. As we will see in the next

section, even without resorting to continuous monitoring in time, lifting these two constraints already allows one for some nontrivial improvements on the minimum error probability value.

Let us now address the QBT problem and continuous-monitoring assumptions. As described in [59], in this case the hypothesis testing can follow two different approaches: In order to discriminate between the two hypotheses, one may exploit the continuous experimental data D_t only or one can also implement a final direct measurement on S and A_1 on the corresponding conditional states. We now start to assess the first scenario. In this case one can resort to a Bayesian analysis, by first observing that each trajectory D_t is characterized by a probability $P(D_t|q)$, when conditioned on the initial assumption that the bath is defined by a statistics associated with the QBT hypothesis q. Hence, introducing a likelihood $L(D_t|q) = P(D_t|q)/p_0(D_t)$, with $p_0(D_t)$ denoting a positive function of D_t only [59], and by resorting to Bayes theorem, it is possible to compute the *a posteriori* probability as

$$P(q|D_t) = \frac{P(D_t|q)}{\sum_{q'} P(D_t|q')} = \frac{L(D_t|q)}{\sum_{q'} L(D_t|q')}, \tag{12}$$

which we present here exploiting the fact that the prior distribution on q is flat [the specific definition of $L(D_t|q)$ and the method to efficiently compute it is discussed in detail in Appendix A]. Observe next that as (12) is normalized for each value of the QBT hypothesis index q we have two possibilities, namely, $P(q|D_t) > \frac{1}{2}$, in which case the bath is most likely to be of q nature, and $P(q|D_t) < \frac{1}{2}$, in which the opposite hypothesis is more plausible. However, the inherent stochasticity of the measurement outcomes can result in $P(B|D_t) \geqslant \frac{1}{2}$ [$P(F|D_t) \geqslant \frac{1}{2}$] even if the statistics of the bath is fermionic (bosonic), i.e., there are measurement records that may lead to a wrong inference process. The goal is thus to quantify the probability of occurrence of such wrong tagging events. In the spirit of a thought experiment, we consider a sample of $N_{\rm traj}$ trajectories D_t, supposing that half of them are generated by indirectly probing a bosonic environment (D_t^B), while the rest are fermionic (D_t^F). A wrong tagging event is triggered every time we have a trajectory D_t^q such that $P(q|D_t^q) < \frac{1}{2}$. Counting the number $N_{\rm wrong}$ of such trajectories leads to the first way to quantify the error probability as the ratio

$$p_{\rm err}^{(\rm cont)}[t;\hat{\varrho}(0)] := \frac{N_{\rm wrong}}{N_{\rm traj}}, \tag{13}$$

where the notation stresses the implicit dependence upon the specific choice of the input state $\hat{\varrho}(0)$ of SA_1 and on the total evolution time t.

As mentioned before, a discrimination capability higher than (13) can in principle be achieved by improving our continuous-monitoring scheme with the addition of a Helstrom projective measurement on S and A_1 at the final time t. In this case the ultimate bound for the error probability is given by the general Helstrom bound in Eq. (10), for the two quantum states $\hat{\varrho}_{B,F}^c(t)$, solutions of the SME (4) or (6) for the data set D_t, and obtained numerically via Eq. (A1), with prior probabilities $P(q|D_t)$. We obtain the nonlinear functional of the detector records

$$\epsilon^c[t;\hat{\varrho}(0)] := \frac{1 - \|P(F|D_t)\hat{\varrho}_F^c(t) - P(B|D_t)\hat{\varrho}_b^c(t)\|_1}{2}. \tag{14}$$

We remark that, apart from influencing the dynamics of the density matrices $\hat{\varrho}_B^c(t)$ and $\hat{\varrho}_F^c(t)$, the knowledge coming from continuous monitoring updates the two prior probabilities [59] and in general identifies the optimal Helstrom projective measurement. An average over all the $N_{\rm traj}$ trajectories of our sample returns the figure of merit

$$p_{\rm err}^{(\rm cont+proj)}[t;\hat{\varrho}(0)] := \mathbb{E}\{\epsilon^c[t;\hat{\varrho}(0)]\}, \tag{15}$$

which thus takes into account the average information gained from both the continuous monitoring and a final Helstrom projective measurement for each trajectory.

III. ANALYSIS AND RESULTS

In this section we present our main results. We start in Sec. III A by discussing the entanglement-assisted QBT scheme obtained by adding the (dynamically neutral) memory element A_1 to the setup of Ref. [22]. In Sec. III B we characterize the advantages one can get by noise-assisted QBT schemes associated with the presence of interaction between S and the auxiliary bath A. Finally, in Sec. III C we address the continuous-monitoring QBT scenario, where part of the information dissipated by S into A is detected in real time via homodyne or photocounting measurements.

A. Advantage of initial entanglement

From the results of Refs. [2,25–31] we expect that the performances of the QBT scheme could benefit by allowing initial correlations between S and the external memory element A_1 and by performing joint measurement on SA_1. The aim of the present section is to verify this expectation. For this purpose let us introduce $\mathcal{E}_{q,t}$, the linear, completely positive, trace-preserving channel [68,69] that allows us to express the solution of Eq. (2) as $\hat{\varrho}_q(t) = \mathcal{E}_{q,t}\hat{\varrho}(0)$. Observe hence that, for fixed t, the minimal value that the HEP of Eq. (11) can attain can be expressed as

$$\epsilon[t;\hat{\varrho}(0)] \geqslant \epsilon_\diamond(t) := \frac{1}{2}\left(1 - \frac{\|\mathcal{E}_{B,t} - \mathcal{E}_{F,t}\|_\diamond}{2}\right), \tag{16}$$

with

$$\|\mathcal{E}_{B,t} - \mathcal{E}_{F,t}\|_\diamond := \max_{\hat{\varrho}(0)\in\mathfrak{S}_{SA_1}} \|\mathcal{E}_{B,t}\hat{\varrho}(0) - \mathcal{E}_{F,t}\hat{\varrho}(0)\|_1 \tag{17}$$

the diamond-norm distance [70,71] obtained by maximizing over the set $\mathfrak{S}_{SA_1}$ of the input joint density matrices of S and A_1. According to Eq. (10), the term $\epsilon_\diamond(t)$ of (16) represents the minimal QBT error probability we can get when performing joint measurements on SA_1 after the probe S has interacted with E for a time t. This term should be compared with the quantity

$$\epsilon_1(t) := \frac{1}{2}\left(1 - \frac{\|\mathcal{E}_{B,t} - \mathcal{E}_{F,t}\|_1}{2}\right), \tag{18}$$

with

$$\|\mathcal{E}_{B,t} - \mathcal{E}_{F,t}\|_1 := \max_{\hat{\varrho}(0)\in\mathfrak{S}_S} \|\mathcal{E}_{B,t}\hat{\varrho}(0) - \mathcal{E}_{F,t}\hat{\varrho}(0)\|_1, \tag{19}$$

which represents instead the optimal QBT error probability one can get by restricting the analysis to only local density matrices of S as assumed in Refs. [22,23]. The fact that using A_1 can provide better QBT performances then follows simply by the natural ordering between the diamond-norm distance and the corresponding trace-norm distance [68], which implies $\|\mathcal{E}_{B,t} - \mathcal{E}_{F,t}\|_\diamond \geqslant \|\mathcal{E}_{B,t} - \mathcal{E}_{F,t}\|_1$, and hence

$$\epsilon_1(t) \geqslant \epsilon_\diamond(t). \tag{20}$$

It is worth stressing that the above inequality applies irrespective of the presence of the coupling with the extra bath A. To quantitatively evaluate the advantages implied by this effect, we now focus on the special scenario where A is disconnected (i.e., $\kappa = 0$) and the temperatures of E in the two QBT hypotheses are the same, i.e., $\beta_B = \beta_F = \beta$, and sufficiently large, i.e., $\beta \to 0$. Under these conditions, the rescaled rate constants corresponding to the bosonic hypothesis, i.e., $q = B$, diverge, while those for the fermionic hypothesis, i.e., $q = F$, remain finite. As a consequence, the bosonic channel $\mathcal{E}_{B,t}$ will imply immediate thermalization of S, in the sense that it leads to thermalization of the probe system on timescales τ where the fermionic channel $\mathcal{E}_{F,t}$ has not significantly affected the dynamics yet, i.e., formally

$$\mathcal{E}_{B,\tau}\bullet \simeq \hat{\varrho}_\beta \otimes \mathrm{Tr}_S[\bullet], \quad \mathcal{E}_{F,\tau}\bullet \simeq \mathcal{I}\bullet, \tag{21}$$

where

$$\hat{\varrho}_\beta := \exp(-\beta \hat{H}_S)/\mathrm{tr}[\exp(-\beta \hat{H}_S)] \tag{22}$$

is the Gibbs thermal state of the probe, $\mathrm{Tr}_S[\bullet]$ represents the partial trace with respect to S, and $\mathcal{I}$ is the identity superoperator. Choosing hence the initial state $\hat{\varrho}(0)$ of S and A_1 to be the maximally entangled state

$$|\Phi^+\rangle := (|11\rangle_{SA_1} + |00\rangle_{SA_1})/\sqrt{2}, \tag{23}$$

from (11) we get

$$\begin{aligned}\|\mathcal{E}_{B,\tau}\hat{\varrho}(0) - \mathcal{E}_{F,\tau}\hat{\varrho}(0)\|_1 &\simeq \left\|\hat{\varrho}(0) - \hat{\varrho}_\beta \otimes \frac{\mathbb{1}}{2}\right\|_1 \\ &\simeq \left\||\Phi^+\rangle\langle\Phi^+| - \frac{\mathbb{1}}{2}\otimes\frac{\mathbb{1}}{2}\right\|_1 = \frac{3}{2},\end{aligned} \tag{24}$$

where in the second line we invoke the limit $\beta \to 0$ to approximate $\hat{\varrho}_\beta \simeq \mathbb{1}/2$. Substituting this into Eq. (11) gives finally

$$\epsilon(\tau; |\Phi^+\rangle) \simeq \tfrac{1}{8}, \tag{25}$$

which by construction provides an upper bound for the optimal entanglement-assisted minimal QBT error probability $\epsilon_\diamond(\tau)$, i.e.,

$$\tfrac{1}{8} \gtrsim \epsilon_\diamond(\tau). \tag{26}$$

Consider next what happens if we eliminate A_1 from the problem, i.e., force $\hat{\varrho}(0)$ to be a local density matrix of just S. Under this circumstance, Eq. (24) gets replaced by

$$\|\mathcal{E}_{B,\tau}\hat{\varrho}(0) - \mathcal{E}_{F,\tau}\hat{\varrho}(0)\|_1 \simeq \|\hat{\varrho}(0) - \hat{\varrho}_\beta\|_1 \simeq \left\|\hat{\varrho}(0) - \frac{\mathbb{1}}{2}\right\|_1 \leqslant 1, \tag{27}$$

with the last inequality being reachable by taking $\hat{\varrho}(0)$ pure, e.g., the vector $|1\rangle$. Accordingly, we can write

$$\epsilon_1(\tau) = \epsilon(\tau; |1\rangle) \simeq \tfrac{1}{4}, \tag{28}$$

which is twice the upper bound (26) on the entanglement-assisted minimal QBT error probability $\epsilon_\diamond(\tau)$ attainable by using correlated input for S and A_1. Finally, we note that the bound (27) applies to any separable input state too, proving the usefulness of the initial entanglement.

B. Noise-assisted QBT

In this section we show how the mere presence of the auxiliary bath A can improve the QBT performances. In order to exclude spurious effects associated with the auxiliary memory element A_1 we focus on the steady-state regime ($t \to \infty$) where the details of the initial state of S and A_1 are not relevant. Since no continuous monitoring of the system is considered at this level, as in the preceding section the equation of motion of the model is still provided by Eq. (2), which we study in the two alternative scenarios where the coupling with A is active ($\kappa \neq 0$) or switched off ($\kappa = 0$). As we will see, the QBT advantages we get in the first case can be traced back to the fact that adding A to the picture [i.e., passing from $\kappa = 0$ to $\kappa \neq 0$ in Eq. (2)] modifies the dynamical process which is responsible for the encoding of the statistical nature of E on the SA_1 system. While in a generic metrology setting there is no guarantee that such interference will have positive effects, the theory does not preclude this for some special tasks: The QBT problem we present here is one such special example.

To help explain the possibility of exploiting the mere presence of A to boost the QBT performances it is useful to consider the scenario where the two QBT hypotheses are characterized by the same temperature (i.e., $\beta_B = \beta_F = \beta$): Under this condition for t sufficiently large, the contact with E alone ($\kappa = 0$) will lead S to the Gibbs state (22), regardless of the nature of the bath, hence making the QBT discrimination impossible [22]. Yet there is a chance that by taking $\kappa \neq 0$ the simultaneous interactions of S with E and A will interfere, leading to departures from such dead-end behavior paving the way for improvements of the discrimination efficiency even for large t (it is also clear, however, that one could also expect that in order to be beneficial, such deviations should not be too strong so that the S-E coupling gets completely dominated by the S-A interaction). To see this explicitly, let us study the values that the HEP figure of merit $\epsilon[t; \hat{\varrho}(0)]$ of Eq. (11) attains in the asymptotic regime of $t \to \infty$ as a function of κ, considering the scenario where the S-A interaction is mediated by the operator $\hat{c} = \hat{\sigma}_-$ (dissipative coupling). In this case, irrespective of the choice of the initial state $\hat{\varrho}(0)$ of S and A_1, we obtain the steady-state HEP value

$$\epsilon(t \to \infty) = \frac{1}{2} - \frac{1}{2\omega_0\kappa}\left|\dot{Q}^{(E_B \Rightarrow A)} - \dot{Q}^{(E_F \Rightarrow A)}\right|, \tag{29}$$

which by construction coincides with $\epsilon_\diamond(\infty)$ and $\epsilon_1(\infty)$. In the above expression $\dot{Q}^{(E_q \Rightarrow A)}$ denotes the heat flows from E to A associated with the QBT hypotheses

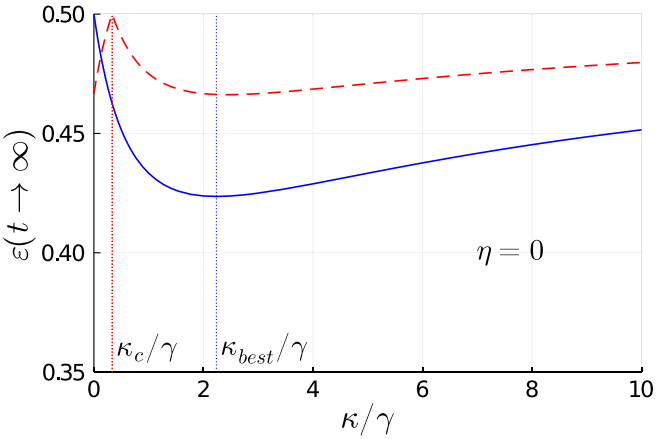

FIG. 2. Plot of the noise-assisted Helstrom bound $\epsilon(t\to\infty)$ reported in Eq. (29), as a function of κ/γ, considering the jump operator $\hat{c}=\hat{\sigma}_-$. No continuous monitoring of the system is considered at this level ($\eta=0$). The blue solid line shows the isothermal QBT scenario $\beta_B=\beta_F=\beta$ with $N_B(\beta)=2$ and the red dashed line is an example of an asymmetric temperature QBT scenario with $N_B(\beta_B)=1$ and $N_B(\beta_F)=2$. Here we notice that $\epsilon(t\to\infty)$ is smaller than $\frac{1}{2}$ for $\kappa=0$, reaching instead the zero discrimination threshold at an intermediate critical value determined by Eq. (32).

$q=B,F$, i.e., the quantities

$$\dot{Q}^{(E_B\Rightarrow A)}=\omega_0\kappa\frac{N_B(\beta_B)}{1+2N_B(\beta_B)+\kappa/\gamma},$$
$$\dot{Q}^{(E_F\Rightarrow A)}=\omega_0\kappa\frac{N_B(\beta_F)}{1+2N_B(\beta_F)+[1+2N_B(\beta_F)]\kappa/\gamma}, \quad (30)$$

which we report here for arbitrary choices of β_B and β_F. The result (29) holds also for the case $\hat{c}=\hat{\sigma}_x/2$, up to a numerical factor and different expressions for the heat flows (see Appendix B for the derivation of all the results). As anticipated, we note that for $\beta_B=\beta_F=\beta$ and $\kappa=0$, one gets $\epsilon(t\to\infty)=\frac{1}{2}$, signaling the impossibility of solving the QBT problem [22]. We observe also that for $\kappa\gg\gamma$ one has $\epsilon(t\to\infty)=\frac{1}{2}$, signaling that the large disturbance originated by A nullifies the sensitivity to the statistics of the bath E. Most interestingly, however, when κ is finite we get a clear advantage with respect to the $\kappa=0$ case (see Fig. 2). The physical interpretation of such noise-assisted QBT improvement is that since A is a zero-temperature bath there is finite average heat flowing from the hot bath E with $q=B,F$ that can be monitored by the probe; the nonzero discrimination capability hence follows due to the fact that a fermionic E implies a slower heat transfer from E to S than a bosonic E. Figure 2 also makes evident that there exists in particular an optimal coupling constant κ minimizing (29), which for $\hat{c}=\hat{\sigma}_-$ can be analytically evaluated as

$$\kappa_{\rm best}/\gamma=\sqrt{2N_B(\beta)+1} \quad (31)$$

[when the S-A is mediated by the operator $\hat{c}=\hat{\sigma}_x/2$ the optimal value is twice that above (see Appendix B)].

A similar analysis can also be conducted for the case of asymmetric temperatures ($\beta_B\neq\beta_F$); here, however, the model naturally allows also for discrimination at steady state also in the case $\kappa=0$, as already studied in [23]. Accordingly, while in some regimes one can still get improvements by working with $\kappa\neq0$, the study become slightly more involved and possibly less interesting. Instead, considering again $\hat{c}=\hat{\sigma}_-$ coupling, we would like to report the fact that in this unequal temperature scenario there can be critical κ values

$$\frac{\kappa_c}{\gamma}=\frac{N_B(\beta_F)-N_B(\beta_B)}{N_B(\beta_B)[1+2N_B(\beta_F)]-N_B(\beta_F)} \quad (32)$$

where QBT discrimination is made impossible [i.e., $\epsilon(t\to\infty)=\frac{1}{2}$] by the presence of A (see the dashed line in Fig. 2). This is actually happening if and only if we have either

$$\tfrac{1}{2}<N_B(\beta_B)<N_B(\beta_F) \quad (33)$$

or

$$N_B(\beta_B)<N_B(\beta_F)<\frac{N_B(\beta_B)}{1-2N_B(\beta_B)}. \quad (34)$$

This last property marks a difference of the noise-assisted QBT with $\hat{c}=\hat{\sigma}_x/2$, where a nonzero discrimination capability at steady state for κ finite may occur but the critical points appear only for $N_B(\beta_B)\geqslant N_B(\beta_F)$ (see Appendix B). In summary, the additive noise implied by an engineered additional environment can on the one hand open the discrimination window for two baths at the same temperature or on the other hand prevent discrimination of two baths at different temperatures when choosing "unlucky" values of the loss coefficient.

C. Monitoring-enhanced QBT

We now discuss the performance in the QBT protocol when the additional environment can be continuously monitored, by considering the two scenarios corresponding to either fluorescence or dispersive monitoring corresponding to the jump operators $\hat{c}=\hat{\sigma}_-$ or $\hat{c}=\hat{\sigma}_x/2$, respectively. We recall that under these circumstances the system dynamics is described by the SME (4) or (6), depending on the type of measurements we have selected and that the attainable mean error probability can be evaluated either in terms of the functional $p_{\rm err}^{(\rm cont)}[t;\hat{\varrho}(0)]$ of Eq. (13) or in terms of its improved version $p_{\rm err}^{(\rm cont+proj)}[t;\hat{\varrho}(0)]$ of Eq. (15), depending on whether or not we allow for a final Helstrom measurement on SA_1. In an effort to simplify the study in what follows we will fix as input state for SA_1 the maximally entangled state (23), the only exception being for the data reported in Fig. 3(a), where we assume S to be uncorrelated with A_1. While in principle for given t this is possibly not the optimal choice in terms of the diamond-norm requirement, the choice is an educated guess as its evolved counterpart is nothing but the Choi-Jamiołkowski state [68,69] of the associated dynamical map that is known to provide a faithful representation of the map itself.

1. Purely dissipative S-A coupling regime

Here we focus on the case where S and A interact through the jump operator $\hat{c}=\hat{\sigma}_-$. The usefulness of exploiting the knowledge deriving from the continuous monitoring of A is highlighted in Fig. 3, where for brevity we only focus on homodyne detection. In this figure the quantity $p_{\rm err}^{(\rm cont+proj)}(t)$ is plotted as a function of t for different choices of the quantum efficiency η. As intuitively expected, increasing η

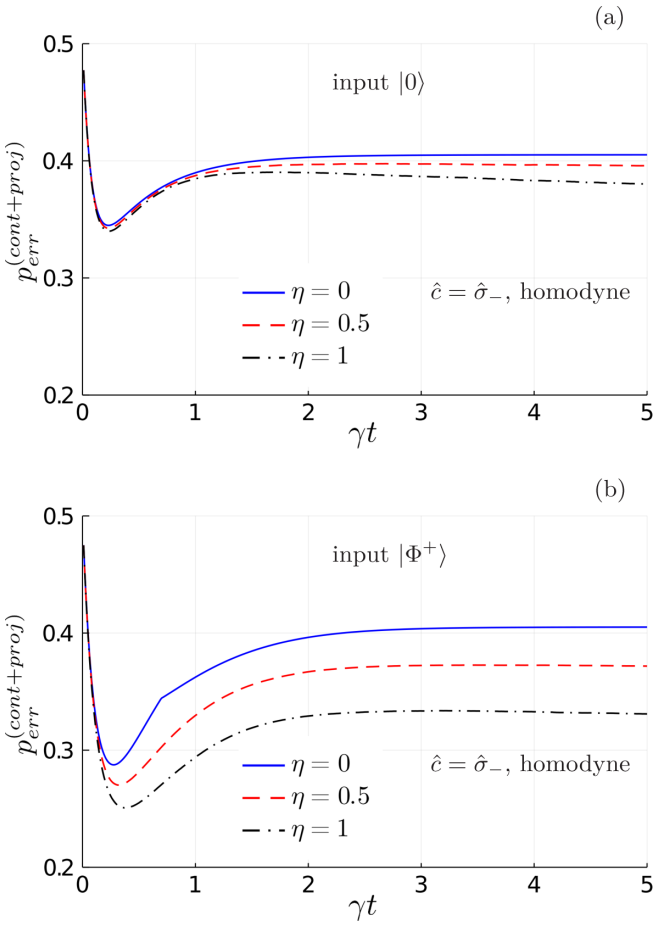

FIG. 3. Plot of $p_{\rm err}^{(\rm cont+proj)}$ [Eq. (15)] in the case of homodyne detection for the different values of the efficiency η given in the legend. (a) The input state of S is the ground state of its local Hamiltonian. (b) Maximally entangled state $|\Phi^+\rangle$ as the input of S and A_1. All data in the figure are obtained in the isothermal QBT scenario $\beta_B = \beta_F = \beta$ for $\beta\omega_0 = 1/5.5$ and $\kappa/\gamma = 1$ and considering the jump operator $\hat{c} = \hat{\sigma}_-$.

leads to better discrimination performance. In particular, the worst-case scenario is obtained for $\eta = 0$ (blue curves in the plot, corresponding to the noise-assisted strategy where we do not monitor A), while the best case is associated with $\eta = 1$ (black dash-dotted curve, corresponding to perfect detection efficiency).

We then fix the monitoring efficiency to its maximum value $\eta = 1$ and turn our attention to the coupling κ that gauges the S-A coupling, which in this framework can be interpreted also as a measurement strength. The results are depicted in Figs. 4(a), 4(b), 4(d), and 4(e), where in Figs. 4(a) and 4(b) [Figs. 4(d) and 4(e)] we show the behavior of $p_{\rm err}^{(\rm cont)}(t)$ [$p_{\rm err}^{(\rm cont+proj)}(t)$] for different values of κ. The first thing one may notice is that for low values of κ photodetection is less efficient than homodyne in reducing $p_{\rm err}^{(\rm cont)}(t)$, while for large values of κ it becomes the preferable choice [see Figs. 4(a) and 4(b)]. Regarding $p_{\rm err}^{(\rm cont+proj)}(t)$ independently of the type of detection on A, we can make two relevant observations: (i) At short timescales the monitoring of A does not lead to a better discrimination as indeed the optimal value still corresponds to the case $\kappa = 0$ (blue curves in the figure); (ii) on the other hand, at long timescales the cumulative information acquired by continuous monitoring definitely improves discrimination for increasing values of κ. In particular, we have numerical evidence that both $p_{\rm err}^{(\rm cont)}(t)$ and $p_{\rm err}^{(\rm cont+proj)}(t)$ go to zero in the long-time limit and thus that in general the minimum error probability obtainable for $\kappa = 0$ can be overcome by considering either κ and/or time long enough (see Fig. 5).

2. Dispersive S-A coupling

Consider next the possibility of coupling dispersively the system to the environment A represented by taking $\hat{c} = \hat{\sigma}_x/2$ as the jump operator of the model [63]. We start by observing that, as $\hat{c}^\dagger\hat{c} = \hat{\sigma}_x^2/4 = \mathbb{1}/4$, the probability for continuous photodetection is independent of the state and thus it cannot contain any information on the bath E. For this reason, for the photodetection unraveling one would obtain $p_{\rm err}^{(\rm cont)}(t) = \frac{1}{2}$ at any time t. We thus show the result of $p_{\rm err}^{(\rm cont)}(t)$ for homodyne detection only [see Fig. 4(c), with the corresponding case of final projective measurement on SA_1 in Fig. 4(f)]. Also in this case we find that at short timescales the coupling with A and the monitoring are not helpful, as the best performances are observed for $\kappa = 0$. On the other hand, we find that $p_{\rm err}^{(\rm cont+proj)}(t)$ decreases towards zero at long timescales and that, as in the previous case, better results are obtained by increasing the coupling κ. We do not provide results for continuous photodetection with a final projective measurement as, while error probabilities below $\frac{1}{2}$ are observed, the performances are definitely worse with respect to the other cases we have considered.

3. Comparison of strategies

We compare the three different strategies, continuous homodyne detection and photodetection with $\hat{c} = \hat{\sigma}_-$ and continuous homodyne detection with $\hat{c} = \hat{\sigma}_x/2$ in Fig. 5. We observe that in the long-time limit the two best strategies correspond to performing either continuous homodyne detection on an environment coupled dispersively via the jump operator $\hat{c} = \hat{\sigma}_x/2$ or continuous photodetection with jump operator $\hat{c} = \hat{\sigma}_-$. Moreover, the first strategy is also the best one in the short-time limit (we remark that similar results are obtained numerically for different values of the parameters).

As regards the difference between the two homodyne strategies for the dissipative jump operator σ_- and for the dispersive jump operator $\sigma_x/2$, we provide the following interpretation in terms of the generation of coherences in the density operator. First we observe that for both cases, the unconditional evolution we are considering does not create elements of the density operator that are off-diagonal in the σ_z basis. However, for homodyne continuous monitoring to be effective, these components are fundamental: The photocurrent in fact bears information on the average value of the Pauli operator σ_x and thus on those density operator's elements. Referring to Eqs. (5) and (6), we understand that these coherences are indeed created in both the dispersive and the dissipative cases over each trajectory. However, while

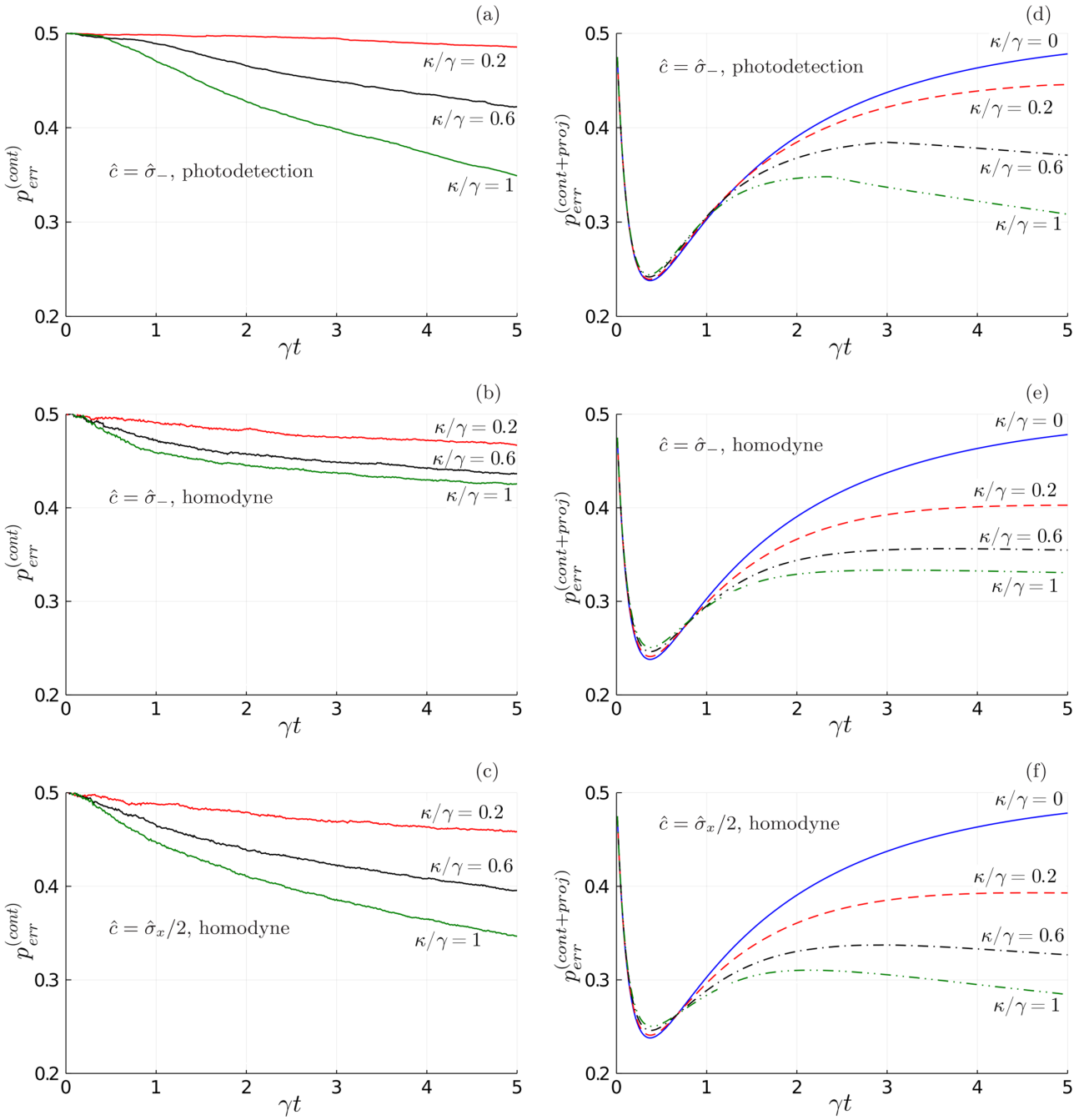

FIG. 4. Setting $|\Phi^+\rangle$ as the initial state of the SA_1 system, we plot (a)–(c) $p_{\rm err}^{(\rm cont)}(t)$ and (d)–(f) $p_{\rm err}^{(\rm cont+proj)}(t)$ for different detection strategies: for $\hat{c} = \hat{\sigma}_-$, (a) and (d) photodetection and (b) and (e) homodyne detection, and for $\hat{c} = \hat{\sigma}_x/2$, (c) and (f) homodyne detection. Different curves refer to different values of κ as indicated in the figure, with $\kappa = 0$ referring to the case where A is decoupled from the probe. All data in this figure are obtained in the isothermal QBT scenario $\beta_B = \beta_F = \beta$, setting $\beta\omega_0 = 1/5.5$ and $\eta = 1$.

with the dissipative coupling σ_- only the part of the density matrix corresponding to the excited state gives a contribution, with the dispersive coupling $\sigma_x/2$, both the ground state and the excited part generate coherences, and the ground state is generally more populated in the trajectories we are considering. In conclusion, dispersive coupling is more effective in creating coherences that are necessary in order to get useful information from the homodyne photocurrent obtained via continuous monitoring, leading to a better discrimination power.

IV. CONCLUSION

In this work we have investigated the possibility of improving the performance of the QBT task originally presented in [22,23] using extra auxiliary resources such as an extra memory element A_1 that could be initially entangled with the original probe S and an extra environment A that is allowed to interact with S while possibly being monitored continuously in time. In particular, we noted that the QBT task can benefit even when A is monitored very inefficiently ($\eta = 0$), an effect

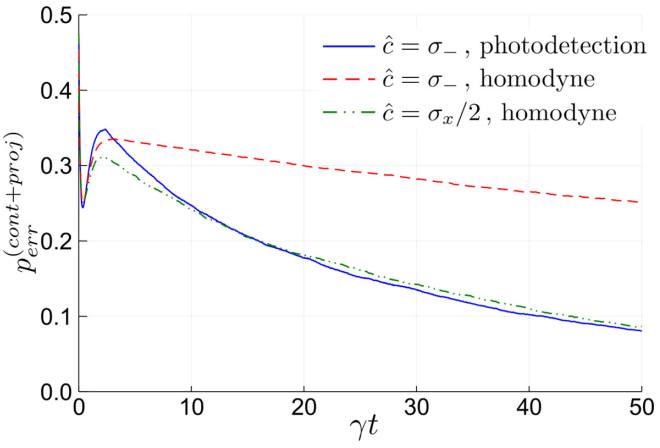

FIG. 5. Long-time behavior of $p_{\rm err}^{(\rm cont+proj)}(t)$ for different continuous-monitoring strategies (see the legend). All data are obtained in the isothermal QBT scenario $\beta_B = \beta_F = \beta$, setting $\beta\omega_0 = 1/5.5$, $\eta = 1$, and $\kappa/\gamma = 1$ and considering $|\Phi^+\rangle$ as the initial state.

that is observed, for instance, in the equal-temperature case which for a long interaction time would not allow for QBT discrimination in the original proposal [22,23]. We finally compared the performances associated with different realizations of continuous monitoring of A via photodetection or homodyne detection, proving that a finite detection efficiency is naturally beneficial to the QBT task. More specifically, numerical simulations show that while for small times the monitoring setup slightly deteriorates the precision given by the sole Helstrom projective scenario (i.e., where the coupling with the bath A is set to zero), by waiting for a long enough time one can achieve a large improvement in the discrimination performance.

Before concluding we would like to comment that the reported results, while derived in the specific QBT setting of [22,23], can be generalized to improve the performances of arbitrary quantum hypothesis tasks, in particular in all those problems where an agent is asked to use an external probe to discriminate between alternative quantum trajectories associated with different dynamical quantum generators. We also would like to mention that experimental realizations for the specific setup we have analyzed in this paper are feasible, e.g., in the context of superconducting qubits [63,72]. In these models, assuming S and A_1 to be superconducting transmon qubits, the initial entanglement configuration between them can be reached, for example, with the use of a common bus resonator [73]. Note also that configurations where S is capacitively coupled with two baths E and A (the latter being continuously monitored) are now experimentally under control, e.g., interpreting the S as a quantum valve [74]. In particular, in our case the engineered environment A may consist in a cavity where this time only S is embedded and the initial coupling with A_1 is now off-detuned, and the transmission of input microwave fields is used for quadrature and dispersive measurements [75]. Specifically, either a fluorescence measurement [72], corresponding to a jump operator $\hat{c} = \hat{\sigma}_-$, or a dispersive measurement [63], corresponding, for example, to a jump operator $\hat{c} = \hat{\sigma}_x/2$, is performed by using a resonant field. The output for homodyne measurement is instead recorded via a Josephson parametric amplifier or, in the case of heterodyne measurements, via a Josephson parametric converter [72]. The final Helstrom measurement on SA_1 can be generally achieved in these experiments by applying a strong dispersively coupled probe field [59,75,76].

ACKNOWLEDGMENTS

We thank Antonio Acín for feedback and inspiration. D.F. acknowledges support from the Government of Spain (FIS2020-TRANQI and Severo Ochoa CEX2019-000910-S), Fundació Cellex, Fundació Mir-Puig, Generalitat de Catalunya (CERCA program) and from the ERC AdG CERQUTE. V.C. acknowledges the National Research Fund of Luxembourg for support through Project QUTHERM C18/MS/12704391. M.G.G. acknowledges the UniMi—Piano di Sostegno alla Ricerca 2020 initiative for support. V.G. acknowledges Ministero dell'Istruzione, Università e della Ricerca for support via project PRIN 2017 Taming complexity via QUantum Strategies a Hybrid Integrated Photonic approach, Project No. 2017SRNBRK.

APPENDIX A: NUMERICAL INTEGRATION OF STOCHASTIC MASTER EQUATIONS

We describe here the method proposed in [66,67] in order to efficiently integrate numerically SMEs, such as Eqs. (4) and (6). The quantum state solution of these SMEs can be written after each time step dt as

$$\hat{\varrho}_q^c(t+dt) = \frac{\sum_k \hat{M}_{x_t}^{(k)}[\hat{\varrho}_q^c(t) + \mathcal{L}_q\hat{\varrho}_q^c(t)dt]\hat{M}_{x_t}^{(k)\dagger}}{\mathrm{Tr}\{\sum_k \hat{M}_{x_t}^{(k)}[\hat{\varrho}_q^c(t) + \mathcal{L}_q\hat{\varrho}_q^c(t)dt]\hat{M}_{x_t}^{(k)\dagger}\}}, \tag{A1}$$

where we have introduced the Kraus operators $\hat{M}_{x_t}^{(k)}$ that describe the effect of the measurement, with outcome x_t, on the quantum state at each time t. The form of these operators depends on the kind of measurement that is performed. In the case of photodetection, the two Kraus operators corresponding to the two possible measurement outcomes $x_t = \{0, 1\}$ are

$$\begin{aligned} \hat{M}_0^{(1)} &= \hat{\mathbb{1}} - \frac{\kappa}{2}\hat{c}^\dagger\hat{c}dt, \\ \hat{M}_0^{(2)} &= \sqrt{(1-\eta)\kappa dt}\hat{c}, \\ \hat{M}_1^{(1)} &= \sqrt{\eta\kappa dt}\hat{c}, \end{aligned} \tag{A2}$$

which are applied according to the Poisson increment probabilities $p_0 = 1 - \eta\kappa\mathrm{Tr}(\hat{\varrho}_q^c\hat{c}^\dagger\hat{c})dt$ and $p_1 = \eta\kappa\mathrm{Tr}(\hat{\varrho}_q^c\hat{c}^\dagger\hat{c})dt$. As regards continuous homodyne detection, the continuous outcome corresponds to the photocurrent $x_t = dy_t$ and the corresponding Kraus operators have the form

$$\begin{aligned} \hat{M}_{dy_t}^{(1)} &= \hat{\mathbb{1}} - \frac{\kappa}{2}\hat{c}^\dagger\hat{c}dt + \sqrt{\eta\kappa}\hat{c}dy_t, \\ \hat{M}_{dy_t}^{(2)} &= \sqrt{(1-\eta)\kappa dt}\hat{c}, \end{aligned} \tag{A3}$$

where the randomness of the process is originated by the Wiener increment entering the formula for the photocurrent (7).

This numerical method also allows us to evaluate straightforwardly the likelihood of each trajectory. In fact, at each time step, the likelihood of obtaining the measurement outcome x_t can be evaluated by taking the trace of the operator at the numerator in Eq. (A1), i.e.,

$$l_{x_t} = \mathrm{Tr}[\tilde{\varrho}^c_q(t+dt)], \tag{A4}$$

where

$$\tilde{\varrho}^c_q(t+dt) = \sum_k \hat{M}^{(k)}_{x_t}\big[\hat{\varrho}^c_q(t) + \mathcal{L}_q\hat{\varrho}^c_q(t)dt\big]\hat{M}^{(k)\dagger}_{x_t}. \tag{A5}$$

As remarked in the main text, by assuming that the monitoring starts and stops at times t_0 and t, respectively, each trajectory can be identified by the string of records D_t of Eq. (8). The corresponding likelihood can thus be evaluated as

$$L(D_t|q) = \prod_{t'=t_0}^{t} l_{x_{t'}} = \prod_{t'=t_0}^{t} \mathrm{Tr}\big[\tilde{\varrho}^c_q(t'+dt)\big]. \tag{A6}$$

APPENDIX B: STEADY STATE FOR A MULTICHANNEL MASTER EQUATION

When we are not continuously monitoring the bath A, the dynamical evolution of S is described by the master equation (2) whose dynamical generator is given by the superoperator

$$\begin{aligned}\mathcal{L}^{(\mathrm{ext})}_q\bullet &:= \mathcal{L}_q\bullet + \kappa\mathcal{D}_{[\hat{c}]}\bullet \\ &= -i[\hat{H}_S,\bullet] + \gamma^-_q\mathcal{D}_{[\hat{\sigma}_-]}\bullet + \gamma^+_q\mathcal{D}_{[\hat{\sigma}_+]}\bullet + \gamma^x_q\mathcal{D}_{[\hat{\sigma}_x/2]}\bullet,\end{aligned}$$

where for two cases considered in the main text $\hat{c} = \{\hat{\sigma}_-, \hat{\sigma}_x/2\}$ we have

$$\begin{aligned}&\gamma^-_q = \gamma(1+s_qN_q(\beta_q)) + \kappa, \quad \gamma^+_q = \gamma N_q(\beta_q),\\ &\gamma^x_q = 0 \quad \text{for } \hat{c} = \hat{\sigma}_-,\\ &\gamma^-_q = \gamma(1+s_qN_q(\beta_q)), \quad \gamma^+_q = \gamma N_q(\beta_q),\\ &\gamma^x_q = \kappa \quad \text{for } \hat{c} = \frac{\hat{\sigma}_x}{2}.\end{aligned} \tag{B1}$$

To discuss the statistics tagging in the long-time limit we solve the equation $\mathcal{L}^{(\mathrm{ext})}_q\hat{\varrho}^{\mathrm{SS}}_q = 0$ which, irrespective of the input state of the system, provides the steady-state $\hat{\varrho}^{\mathrm{SS}}_q$ solution of the system dynamics, i.e.,

$$\lim_{t\to\infty}\hat{\varrho}_q(t) = \hat{\varrho}^{\mathrm{SS}}_q. \tag{B2}$$

Writing hence $\hat{\varrho}^{\mathrm{SS}}_q = p_q|1\rangle\langle 1| + (1-p_q)|0\rangle\langle 0| + c_q|0\rangle\langle 1| + c^*_q|1\rangle\langle 0|$, we obtain the conditions

$$p_q = \frac{\gamma^+_q + \gamma^x_q/4}{\gamma^+_q + \gamma^-_q + \gamma^x_q/2}, \quad c_q = 0. \tag{B3}$$

Notice that irrespective of the selected QBT hypothesis, the off-diagonal elements are always null. On the other hand, the associated conditions for the populations at steady state are obtained by plugging (B1) into Eq. (B3):

$$\begin{aligned}p_B &= \frac{\gamma N_B(\beta_B)}{\gamma(2N_B(\beta_B)+1)+\kappa},\\ p_F &= \frac{\gamma N_F(\beta_F)}{\gamma+\kappa} \quad \text{for } \hat{c} = \hat{\sigma}_-,\\ p_B &= \frac{\gamma N_B(\beta_B) + \kappa/4}{\gamma(2N_B(\beta_B)+1)+\kappa/2},\\ p_F &= \frac{\gamma N_F(\beta_F) + \kappa/4}{\gamma+\kappa/2} \quad \text{for } \hat{c} = \frac{\hat{\sigma}_x}{2}.\end{aligned} \tag{B4}$$

With the above expressions we can now express the asymptotic limit of the HEP functional (11)

$$\begin{aligned}\lim_{t\to\infty}\epsilon[t;\hat{\varrho}(0)] &= \epsilon[t\to\infty]\\ &:= \frac{1}{2}\left(1 - \frac{\|\hat{\varrho}^{\mathrm{SS}}_B - \hat{\varrho}^{\mathrm{SS}}_F\|_1}{2}\right)\\ &= \frac{1}{2}(1-|p_B-p_F|).\end{aligned} \tag{B5}$$

We can also represent the figure of merit in terms of the heat flowing between the two environments at steady state. The heat flowing in A is characterized in terms of the equation [77]

$$\dot{Q}^{(E_q\Rightarrow A)} = -\kappa\,\mathrm{Tr}\big(\hat{H}_S\mathcal{D}_{[\hat{c}]}\hat{\varrho}^{\mathrm{SS}}_q\big), \tag{B6}$$

which in the case of $\hat{c} = \hat{\sigma}_-$ gives $\omega_0\kappa p_q$. Combining Eq. (B6) with the first of Eqs. (B4), it is straightforward to obtain the results (29) and (30) of the main text, after expressing the Fermi function in terms of the Bose function for uniforming the notation $N_F(\beta_F) = \frac{N_B(\beta_F)}{1+2N_B(\beta_F)}$. Also in the case of $\hat{c} = \hat{\sigma}_x/2$ we are able to establish a connection between the modulus of the population difference and the heat flow. Using the definition (B6), we have $-\kappa\,\mathrm{Tr}(\hat{H}_S\mathcal{D}_{[\hat{\sigma}_x/2]}\hat{\varrho}^{\mathrm{SS}}_q) = -\frac{\omega_0\kappa}{4}(1-2p_q)$, from which we derive

$$|p_B - p_F| = \frac{2}{\omega_0\kappa}|\dot{Q}^{(E_B\Rightarrow A)} - \dot{Q}^{(E_F\Rightarrow A)}|, \tag{B7}$$

and hence

$$\epsilon[t\to\infty] = \frac{1}{2}\left(1 - \frac{2}{\omega_0\kappa}\big|\dot{Q}^{(E_B\Rightarrow A)} - \dot{Q}^{(E_F\Rightarrow A)}\big|\right). \tag{B8}$$

Finally, we discuss how the tagging procedure can be influenced by the coupling with the bath A, gauged through the parameter κ. Choosing the value of κ for which Eq. (29) is equal to $\frac{1}{2}$ allows us to find κ_c in Eq. (32). The same analysis for the case with $\hat{c} = \frac{\hat{\sigma}_x}{2}$ leads to the critical value

$$\frac{\kappa_c}{\gamma} = 2\frac{N_B(\beta_B)}{N_F(\beta_F)} - 1. \tag{B9}$$

The optimal value for the discrimination at steady state when $\beta_F = \beta_B = \beta$ instead is obtained by optimizing the figures of merit with respect to κ. In this way the results in (31) and

$$\frac{\kappa_{\mathrm{best}}}{\gamma} = 2\sqrt{2N_B(\beta)+1} \tag{B10}$$

are found for $\hat{c} = \hat{\sigma}_-$ and $\hat{c} = \hat{\sigma}_x/2$, respectively.

[1] V. Giovannetti, S. Lloyd, and L. Maccone, Phys. Rev. Lett. **96**, 010401 (2006).
[2] V. Giovannetti, S. Lloyd, and L. Maccone, Nat. Photon. **5**, 222 (2011).
[3] M. G. A. Paris, Int. J. Quantum Inf. **07**, 125 (2009).
[4] R. Demkowicz-Dobrzański, M. Jarzyna, and J. Kołodyński, in *Progress in Optics*, edited by E. Wolf (Elsevier, Amsterdam, 2015), Vol. 60, Chap. 4, pp. 345–435.
[5] C. L. Degen, F. Reinhard, and P. Cappellaro, Rev. Mod. Phys. **89**, 035002 (2017).
[6] S. Pirandola, B. R. Bardhan, T. Gehring, C. Weedbrook, and S. Lloyd, Nat. Photon. **12**, 724 (2018).
[7] M. Mehboudi, A. Sanpera, and L. A. Correa, J. Phys. A: Math. Theor. **52**, 303001 (2019).
[8] T. M. Stace, Phys. Rev. A **82**, 011611(R) (2010).
[9] M. Brunelli, S. Olivares, and M. G. A. Paris, Phys. Rev. A **84**, 032105 (2011).
[10] L. A. Correa, M. Mehboudi, G. Adesso, and A. Sanpera, Phys. Rev. Lett. **114**, 220405 (2015).
[11] M. G. A. Paris, J. Phys. A: Math. Theor. **49**, 03LT02 (2016).
[12] A. De Pasquale, D. Rossini, R. Fazio, and V. Giovannetti, Nat. Commun. **7**, 12782 (2016).
[13] A. De Pasquale, K. Yuasa, and V. Giovannetti, Phys. Rev. A **96**, 012316 (2017).
[14] S. Campbell, M. G. Genoni, and S. Deffner, Quantum Sci. Technol. **3**, 025002 (2018).
[15] A. H. Kiilerich, A. De Pasquale, and V. Giovannetti, Phys. Rev. A **98**, 042124 (2018).
[16] V. Cavina, L. Mancino, A. De Pasquale, I. Gianani, M. Sbroscia, R. I. Booth, E. Roccia, R. Raimondi, V. Giovannetti, and M. Barbieri, Phys. Rev. A **98**, 050101(R) (2018).
[17] S. Razavian, C. Benedetti, M. Bina, Y. Akbari-Kourbolagh, and M. G. A. Paris, Eurp. Phys. J. Plus **134**, 284 (2019).
[18] V. Montenegro, M. G. Genoni, A. Bayat, and M. G. A. Paris, Phys. Rev. Res. **2**, 043338 (2020).
[19] C. Benedetti, F. Salari Sehdaran, M. H. Zandi, and M. G. A. Paris, Phys. Rev. A **97**, 012126 (2018).
[20] M. Bina, F. Grasselli, and M. G. A. Paris, Phys. Rev. A **97**, 012125 (2018).
[21] A. Candeloro and M. G. A. Paris, Phys. Rev. A **103**, 012217 (2021).
[22] D. Farina, V. Cavina, and V. Giovannetti, Phys. Rev. A **100**, 042327 (2019).
[23] I. Gianani, D. Farina, M. Barbieri, V. Cimini, V. Cavina, and V. Giovannetti, Phys. Rev. Res. **2**, 033497 (2020).
[24] C. W. Helstrom, J. Stat. Phys. **1**, 231 (1969).
[25] A. Fujiwara, Phys. Rev. A **63**, 042304 (2001).
[26] G. M. D'Ariano, P. Lo Presti, and M. G. A. Paris, Phys. Rev. Lett. **87**, 270404 (2001).
[27] D. G. Fischer, H. Mack, M. A. Cirone, and M. Freyberger, Phys. Rev. A **64**, 022309 (2001).
[28] F. De Martini, A. Mazzei, M. Ricci, and G. M. D'Ariano, Phys. Rev. A **67**, 062307 (2003).
[29] G. M. D'Ariano and P. Lo Presti, Phys. Rev. Lett. **91**, 047902 (2003).
[30] M. A. Ballester, Phys. Rev. A **69**, 022303 (2004).
[31] A. Smirne, J. Kołodyński, S. F. Huelga, and R. Demkowicz-Dobrzański, Phys. Rev. Lett. **116**, 120801 (2016).
[32] H. M. Wiseman and G. J. Milburn, *Quantum Measurement and Control* (Cambridge University Press, Cambridge, 2009).
[33] K. Jacobs and D. A. Steck, Contemp. Phys. **47**, 279 (2006).
[34] M. Guţă, B. Janssens, and J. Kahn, Commun. Math. Phys. **277**, 127 (2008).
[35] M. Tsang, H. M. Wiseman, and C. M. Caves, Phys. Rev. Lett. **106**, 090401 (2011).
[36] M. Tsang, New J. Phys. **15**, 073005 (2013).
[37] S. Gammelmark and K. Mølmer, Phys. Rev. A **87**, 032115 (2013).
[38] S. Gammelmark and K. Mølmer, Phys. Rev. Lett. **112**, 170401 (2014).
[39] M. Guta and J. Kiukas, J. Math. Phys. **58**, 052201 (2017).
[40] M. G. Genoni, Phys. Rev. A **95**, 012116 (2017).
[41] F. Albarelli, M. A. C. Rossi, M. G. A. Paris, and M. G. Genoni, New J. Phys. **19**, 123011 (2017).
[42] J. Gambetta and H. M. Wiseman, Phys. Rev. A **64**, 042105 (2001).
[43] J. M. Geremia, J. K. Stockton, A. C. Doherty, and H. Mabuchi, Phys. Rev. Lett. **91**, 250801 (2003).
[44] K. Mølmer and L. B. Madsen, Phys. Rev. A **70**, 052102 (2004).
[45] J. K. Stockton, J. M. Geremia, A. C. Doherty, and H. Mabuchi, Phys. Rev. A **69**, 032109 (2004).
[46] M. Tsang, Phys. Rev. A **81**, 013824 (2010).
[47] T. A. Wheatley, D. W. Berry, H. Yonezawa, D. Nakane, H. Arao, D. T. Pope, T. C. Ralph, H. M. Wiseman, A. Furusawa, and E. H. Huntington, Phys. Rev. Lett. **104**, 093601 (2010).
[48] H. Yonezawa, D. Nakane, T. A. Wheatley, K. Iwasawa, S. Takeda, H. Arao, K. Ohki, K. Tsumura, D. W. Berry, T. C. Ralph, H. M. Wiseman, E. H. Huntington, and A. Furusawa, Science **337**, 1514 (2012).
[49] P. Six, P. Campagne-Ibarcq, L. Bretheau, B. Huard, and P. Rouchon, *2015 54th IEEE Conference on Decision and Control* (IEEE, Piscataway, 2015), pp. 7742–7748.
[50] A. H. Kiilerich and K. Mølmer, Phys. Rev. A **94**, 032103 (2016).
[51] L. Cortez, A. Chantasri, L. P. García-Pintos, J. Dressel, and A. N. Jordan, Phys. Rev. A **95**, 012314 (2017).
[52] J. F. Ralph, S. Maskell, and K. Jacobs, Phys. Rev. A **96**, 052306 (2017).
[53] J. Atalaya, S. Hacohen-Gourgy, L. S. Martin, I. Siddiqi, and A. N. Korotkov, npj Quantum Inf. **4**, 41 (2018).
[54] F. Albarelli, M. A. C. Rossi, D. Tamascelli, and M. G. Genoni, Quantum **2**, 110 (2018).
[55] A. Shankar, G. P. Greve, B. Wu, J. K. Thompson, and M. Holland, Phys. Rev. Lett. **122**, 233602 (2019).
[56] M. A. C. Rossi, F. Albarelli, D. Tamascelli, and M. G. Genoni, Phys. Rev. Lett. **125**, 200505 (2020).
[57] A. Fallani, M. A. C. Rossi, D. Tamascelli, and M. G. Genoni, PRX Quantum **3**, 020310 (2022).
[58] M. Tsang, Phys. Rev. Lett. **108**, 170502 (2012).
[59] A. H. Kiilerich and K. Mølmer, Phys. Rev. A **98**, 022103 (2018).
[60] V. Gorini, A. Kossakowski, and E. C. G. Sudarshan, J. Math. Phys. **17**, 821 (1976).
[61] G. Lindblad, Commun. Math. Phys. **48**, 119 (1976).
[62] H.-P. Breuer and F. Petruccione, *The Theory of Open Quantum Systems* (Oxford University Press, Oxford, 2002).
[63] S. Hacohen-Gourgy, L. S. Martin, E. Flurin, V. V. Ramasesh, K. B. Whaley, and I. Siddiqi, Nature (London) **538**, 491 (2016).

[64] A. Chantasri, J. Atalaya, S. Hacohen-Gourgy, L. S. Martin, I. Siddiqi, and A. N. Jordan, Phys. Rev. A **97**, 012118 (2018).
[65] S. Hacohen-Gourgy and L. S. Martin, Adv. Phys.: X **5**, 1813626 (2020).
[66] P. Rouchon, arXiv:1407.7810.
[67] P. Rouchon and J. F. Ralph, Phys. Rev. A **91**, 012118 (2015).
[68] J. Watrous, *The Theory of Quantum Information* (Cambridge University Press, Cambridge, 2018).
[69] A. S. Holevo, *Probabilistic and Statistical Aspects of Quantum Theory*, 2nd ed. (Edizioni della Normale, Pisa, 2011).
[70] A. Y. Kitaev, Russ. Math. Surv. **52**, 1191 (1997).
[71] A. Kitaev, A. Shen, and M. Vyalyi, *Classical and Quantum Computation* (American Mathematical Society, Providence, 2002).
[72] Q. Ficheux, S. Jezouin, Z. Leghtas, and B. Huard, Nat. Commun. **9**, 1926 (2018).
[73] D. J. Egger, M. Ganzhorn, G. Salis, A. Fuhrer, P. Müller, P. K. Barkoutsos, N. Moll, I. Tavernelli, and S. Filipp, Phys. Rev. Appl. **11**, 014017 (2019).
[74] A. Ronzani, B. Karimi, J. Senior, Y.-C. Chang, J. T. Peltonen, C. Chen, and J. P. Pekola, Nat. Phys. **14**, 991 (2018).
[75] D. Tan, S. J. Weber, I. Siddiqi, K. Mølmer, and K. W. Murch, Phys. Rev. Lett. **114**, 090403 (2015).
[76] K. Murch, S. Weber, C. Macklin, and I. Siddiqi, Nature (London) **502**, 211 (2013).
[77] R. Alicki and R. Kosloff, in *Thermodynamics in the Quantum Regime*, edited by F. Binder, L. A. Correa, C. Gogolin, J. Anders, and G. Adesso (Springer, Cham, 2018), Vol. 195, pp. 1–33.